Journal of Materials Chemistry A

Accepted Manuscript

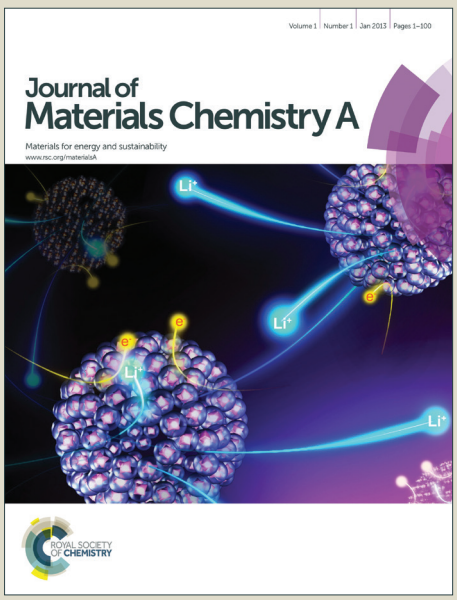

ROYAL SOCIETY OF CHEMISTRY

www.rsc.org/materialsA

A spray drying approach for the synthesis of $Na_2C_6H_2O_4$/CNT nanocomposite anode for sodium-ion batteries

Xiaoyan Wu[1], Jie Ma[1], Qidi Ma[2], Shuyin Xu[1], Yong-Sheng Hu[1], Young Sun[2], Hong Li[1], Liquan Chen[1], Xuejie Huang[1]*

1 Key Laboratory for Renewable Energy, Beijing Key Laboratory for New Energy Materials and Devices, Beijing National Laboratory for Condensed Matter Physics, Institute of Physics, Chinese Academy of Sciences, Beijing 100190, China
E-mail: yshu@aphy.iphy.ac.cn

2 State Key Laboratory of Magnetism and Beijing National Laboratory for Condensed Matter Physics, Institute of Physics, Chinese Academy of Sciences, Beijing 100190, China

Keywords: $Na_2C_6H_2O_4$/CNT, nanocomposite, organic anode, high safety, sodium-ion batteries

Abstract

Sodium-ion batteries have attracted extensive attention for large-scale energy storage applications for renewable energy and smart grid owing to the abundant sodium resources and potential low cost. Comparing with the numerous available cathodes, very few anodes are viable for sodium-ion batteries. Here we report a high-safe and low-cost nanocomposite, disodium 2,5-dihydroxy-1,4-benzoquinone ($Na_2C_6H_2O_4$)/CNT prepared by a simple spray drying method, as high performance anode for sodium-ion batteries. The resulting nanocomposite exhibits a reversible capacity of 259 mAh g^{-1} with first Coulombic efficiency of 88% and excellent rate performance. The average sodium storage voltage is 1.4 V, which prevents the formation of solid electrolyte interphase layer and consequently ensures high safety, high first Coulombic efficiency and superior rate performance.

1. Introduction

Electrochemical energy storage system is one of the most promising means to store electricity in large-scale which is critical for the smooth integration of the renewable intermittent energies, such as wind and solar power, into the grid.[1, 2] Amongst them,

lithium-ion batteries with high energy density have been widely used in portable electronic consumption and would be the best choice for electric vehicles. However, the amount of lithium resources in the Earth's crust would not be sufficient to satisfy the demands of widespread application of electrical vehicles and smart grid simultaneously. Sodium has similar physicochemical properties as lithium and the fundamental principles of lithium-ion batteries and sodium-ion batteries are similar, while the sodium resources are practically inexhaustible. Thus, room-temperature sodium-ion batteries have been recently proposed for these large-scale applications. [3-6]

Safety is another critical factor in such practical application. The lack of anode with appropriate storage voltage impedes the development of high-safety sodium-ion batteries. Numerous carbon-based materials have been studied as anode for sodium-ion batteries. Among them, hard carbon exhibits high storage capacity and good cycling performance. However, the sodium storage voltage of carbon-based materials is close to the sodium plating voltage; on one hand, this will lead to the formation of solid electrolyte interphase (SEI) layer owing to the electrolyte reduction below 0.8 V; on the other hand, this may also cause dendrite growth and consequential safety issues under fast charging or overcharging conditions.[7, 8] Although the storage capacity of several alloys is large, the low first Coulombic efficiency and instable electrode structure caused by large volume change during sodium insertion and extraction make alloys impractical.[9, 10] Ti-based compounds are another important class of anodes which have attracted considerable interest in recent years. It mainly includes Ti-based oxides and Ti-based phosphates $NaTi_2(PO_4)_3$. Ti-based oxides,[11-14] such as $Na_2Ti_3O_7$ and $Na_{0.66}[Li_{0.22}Ti_{0.78}]O_2$, have shown relatively low first Coulombic efficiency due to the formation of a SEI layer, which also influences the high rate performance. Polyanionic $NaTi_2(PO_4)_3$ displays reversible capacity of 120 mAh g^{-1} at 2.1 V via Ti^{4+}/Ti^{3+} conversion. This operating voltage is too positive for high energy density and this material can only be considered with aqueous electrolytes where hydrogen evolution is to be avoided.[15, 16]

Organic electrode materials, which can be obtained from biomass and recyclable resources, are environmentally-friendly and low-cost choices for secondary

batteries.[17-22] Conjugated carbonyl compounds with quinone-type redox centre[23, 24] or carboxyl redox centre[25-27] are important part of organic anode materials with relatively low storage potential. The first reported organic sodium-ion battery anode, disodium terephthalate ($Na_2C_8H_4O_4$), exhibits a high reversible capacity, good cycling performance but low first Coulombic efficiency of 50% due to its low storage voltage.[27-29] It is desired to develop organic anode materials with a storage voltage higher than 0.8 V to avoid the formation of SEI. Dilithium 2,5-dihydroxy-1,4-benzoquinone ($Li_2C_6H_2O_4$) exhibits a lithium storage voltage of 1.6 V.[30] Considering the potential difference between lithium and sodium, this redox centre may provide a proper sodium storage voltage just above 1 V. Moreover, most organics show low electronic and ionic conductivity, which will significantly limit their capacity and rate performance.[31, 32] Thus, organic material must be integrated in efficient charge conduction pathways both in particles and the whole electrode with high surface area. Three-dimensional (3-D) networks of carbon nanotubes electrode structure model can offer high surface area, interpenetrating porosity and efficient charge carrier transport. In addition, porous and hollow structure allows a high contact area of the active material with electrolyte, leading to a fast transport of electrons and sodium ions.

Here, we introduce a $Na_2C_6H_2O_4$/CNT nanocomposite prepared by a simple spray drying method for high-safe sodium-ion batteries, which exhibits a reversible capacity of 259 mAh g^{-1} with excellent rate performance of storage capacity of 142 mAh g^{-1} at 7C (～8 min discharging/charging) rate and first Coulombic efficiency of 88% at an average sodium storage voltage of 1.4 V. The relatively high voltage prevents the formation of SEI layer and dendrites, thereby ensuring a high battery safety. Meanwhile, this spray drying method can be further extended to water- or oil-soluble materials to improve electrode electronic conductivity.

2. Experimental

Synthesis: $Na_2C_6H_2O_4$/CNT nanocomposite sample was synthesized in one step as follow: a stoichiometric amounts of 2,5-Dihydroxy-1,4-benzoquinone (2,5-DBQ)

(TCI, 98%) and NaOH (99%) were dissolved in deionied water, then 10 wt.% hydrophilic carbon nanotubes was added in the solution and dispersed by ultrasound for 3 h. The homogeneous liquid was spray-dried at the inlet and outlet temperatures of 150 °C and 80 °C, respectively. The obtained spherical powders were heated at 300 °C for 4 h in Ar atmosphere. $Na_2C_6H_2O_4$ sample was prepared by a room-temperature liquid-phase reaction between stoichiometric 2,5-DBQ and NaOH. NaOH was dissolved in ethanol and then the solution was slowly injected into a DMSO solution in which 2,5-DBQ was dissolved. An orange precipitate formed and was separated out by centrifugation. The as-obtained powders were washed by ethanol several times, and then dried at 60 °C for 12 h in vacuum.

Characterizations: Powder X-ray diffraction data were collected on a Bruker D8 X-ray diffractometer with Cu Kα radiation (λ = 1.5405 Å) in the scan range of 10-60º. The morphology of the sample was observed by scanning electron microscopy (Hitachi S-4800). EPR spectra were recorded at room temperature with a JEOL JES-FA200 spectrometer. Microwave power and modulation amplitude were respectively set to 1 mW and 0.35 mT.

Electrochemistry: $Na_2C_6H_2O_4$/CNT nanocomposite electrode was fabricated by compressing a mixture of $Na_2C_6H_2O_4$/CNT (53wt.%), acetylene black (42wt.%), and polytetrafluoroethylene (PTFE) binder (5wt.%). The control $Na_2C_6H_2O_4$ electrodes were prepared by mixing $Na_2C_6H_2O_4$ (47wt.%), acetylene black (48wt.%), polytetra-fluoroethylene (5wt.%) homogeneously. The working electrodes were dried at 100 ^oC under vacuum for 10 h. The CR2032 coin-type cells were assembled with pure sodium foil as the counter electrode, and glass fibre as the separator in an argon-filled glove box. The electrolyte is 0.8 M $NaPF_6$ in PC. The discharge and charge measurements were carried out on a Land BT2000 battery test system (Wuhan, China) in a voltage range of 1.0-2.0 V under room temperature.

3. Results and discussion

$Na_2C_6H_2O_4$/CNT composite material was synthesized by means of spray drying with 10 wt.% CNT. Spray drying is widely used for spherical shape granulating in industry

and the process is presented in Figure 1a. The raw material is $Na_2C_6H_2O_4$ aqueous solution containing homodispersed hydrophilic carbon nanotubes. During spray drying, the solute $Na_2C_6H_2O_4$ separates out upon water evaporation, and then forms nanocomposite microparticles together with carbon nanotubes. The formed microparticle is interspersed with carbon nanotubes, as illustrated in Figure 1b. This approach takes the advantage of uniform dispersion of hydrophilic carbon nanotubes to composite with soluble low electronic conductive materials, building conducting network and granulating spheres simultaneously. Either water- or oil-soluble materials are applicable to this approach with carbon nanotubes possessing hydrophilicity or hydrophobicity after different surface modifications. For comparison, we also prepared $Na_2C_6H_2O_4$ by a simple liquid phase reaction using precursors of 2,5-dihydroxy-1,4-benzoquinone (2,5-DBQ) and NaOH in organic solvent at room temperature. X-ray diffraction (XRD) powder patterns collected for $Na_2C_6H_2O_4$ and $Na_2C_6H_2O_4$/CNT nanocomposite samples are showing in Figure 2a and 2b. The $Na_2C_6H_2O_4$ sample prepared from liquid phase reaction crystallizes in space group of *P-1*. However, after spray drying, the pattern of $Na_2C_6H_2O_4$/CNT nanocomposite shows wide full widths at half-maximum, indicating the crystallinity decreases in this process. Meanwhile, the nanocomposite displays (100)-preferential orientation. The morphology of $Na_2C_6H_2O_4$/CNT nanocomposite was investigated with scanning electron microscopy (SEM). As shown in Figure 3, the nanocomposite particles are composed by nanoparticles around 50 nm and in whole show irregular spherical shape with particle size of 1-5 μm. It can be seen that in this porous sphere structure, carbon nanotubes interlace inside the particle and protrude outwards from the sphere surface to build a conductive network in and between microparticles, as illustrated in Figure 1b. The pore size distribution was obtained from the N_2 sorption isotherm through the Barrett–Joyner–Halenda (BJH) approach. The $Na_2C_6H_2O_4$/CNT sample shows typically porous structure with a large number of pores in the range of 40-50 nm. For $Na_2C_6H_2O_4$ sample synthesized in organic solvent, the SEM image shows the particle size in the range of 50-100 nm.

The sodium storage performance of the $Na_2C_6H_2O_4$ electrode and $Na_2C_6H_2O_4$/CNT

electrode in sodium half-cells are shown in Figure 4a and 4b, respectively. For the $Na_2C_6H_2O_4$ electrode, there is one flat plateau at 1.2 V in the first discharge process, showing a two-phase reaction happened with sodium insertion into this structure, while the following charge process presents two voltage plateaus at 1.3 V and 1.6 V. The first discharge capacity is 288 mAh g^{-1} at a current rate of C/10 (C/10 means 2 mol Na insertion into 1 mol $Na_2C_6H_2O_4$ in 10 h), corresponding to two sodium insertion per formula unit. Combining with the charge capacity of 265 mAh g^{-1}, the asymmetric reaction in the first cycle exhibits a Coulombic efficiency of 92%, which is much higher than any other reported organic carbonyl anodes for sodium-ion batteries. It can be attributed to the high storage voltage avoiding SEI formation and sodium consumption. However, the capacity of $Na_2C_6H_2O_4$ electrode fades rapidly. The capacity decreases to 140 mAh g^{-1} in the 5th cycle, and further decreases to 40 mAh g^{-1} in the 10th cycle, which might be ascribed to the low electrical conductivity of this organic material.

The first discharge/charge curves of the $Na_2C_6H_2O_4$/CNT electrode show a reversible capacity of 259 mAh g^{-1} with first Coulombic efficiency of 88%, which are close to that of $Na_2C_6H_2O_4$ electrode and superior to most of other anode materials for sodium-ion batteries. Attributed to the electronic network building by the carbon nanotubes inside and sticked out, the cycle performance of this nanocomposite is significantly improved. After 10 cycles, the capacity remains at 250 mAh g^{-1}. The cyclic voltammetry (CV) curves of $Na_2C_6H_2O_4$/CNT sample are displayed in Figure 4c in the voltage range of 0.8-2.0 V vs. Na^+/Na at a scanning rate of 0.03 mV s^{-1}. One cathodic peak was observed at about 1.15 V on the first negative sweep, corresponding to the reduction of two quinone groups to sodium phenoxide.[30] In the subsequent positive sweep, there are two anodic peaks centred at 1.35 V and 1.65 V, suggesting that the oxidation of sodium phenoxide is a two-step process. From the second cycle, two pairs of redox peaks present in both negative and positive sweeps, which is in good agreement with the discharge/charge curves. These observations indicate that mechanism of the first discharge process is different from the following. Thereafter, the electrode reaction shows high reversibility, thus ensuring good cycle

performance.

To investigate the reaction mechanism, electron paramagnetic resonance (EPR) method was carried out for $Na_2C_6H_2O_4$ samples at different discharge/charge states at room temperature. As shown in Fig. 5, the pristine $Na_2C_6H_2O_4$ material shows no signal as expected due to the even number of electrons. Surprisingly, after discharged to 1 V (corresponding to 2 Na insertion), the discharged $Na_4C_6H_2O_4$ phase shows the onset of a strong isotropic EPR signal (g = 1.9675), indicating that the $Na_4C_6H_2O_4$ phase is in a triplet ground state.[25, 33] Once charged to 1.4 V (corresponding to 1 Na extraction), the EPR spectrum of the charged $Na_3C_6H_2O_4$ phase has a different g value of 1.9685, suggesting the presence of free radicals in $Na_3C_6H_2O_4$ phase. Upon further charged to 2.0 V, the spectrum is similar to the pristine $Na_2C_6H_2O_4$ molecular, showing a high reversibility of the electrode reaction.

The rate capability of the $Na_2C_6H_2O_4$/CNT electrode was also evaluated in a sodium cell. It can be seen from Figure 6a that the reversible capacities are 258, 239, 234, 212, 197, 161 and 142 mAh g^{-1} at current rates of C/10, C/5, C/2, 1C, 2C, 5C and 7C, respectively. The capacity retention at 7C rate (～8 min discharging/charging) is 55% of the initial capacity. As it is well known, SEI layer formed on electrode surface results in large impedance increase. $Na_2C_6H_2O_4$ with high storage voltage has no SEI layer on the surface and hence exhibits superior rate performance. Furthermore, the unique porous structure of favorable transport characteristics builds up a mixed conducting 3-D network for both Na+ ion and electron. The well-connected carbon nanotubes provide a continuous electronic pathway and simultaneously the porous structure makes the liquid electrolyte facile diffusion into the bulk of the electrode material. Moreover, the primary nanoparticles greatly reduce the solid-state transport lengths for Na^+ ion diffusion which is assumed to determine the overall rate in this nanocomposite. Figure 6b shows the capacity and Coulombic efficiency of the $Na_2C_6H_2O_4$/CNT electrode versus cycle number. After 30 cycles, the reversible capacity is still kept at 191 mAh g^{-1} at a current rate of 1C. The capacity retention is 92%. Meanwhile, after initial cycle, the Coulombic efficiency can reach over 99%. It may be due to the porous structure which buffers well against the local volume

change during the Na insertion/extraction and thus enhances the structural stability.

4. Conclusion

In conclusion, the $Na_2C_6H_2O_4$/CNT nanocomposite obtained by a spray drying method shows a reversible capacity of 259 mAh g^{-1} with a high first Coulombic efficiency of 88% and superior rate performance of storage capacity of 142 mAh g^{-1} at 7C rate (～8 min discharging/charging). This nanocomposite exhibits an average sodium storage voltage of 1.4 V free of SEI layer formation and dendrite deposition, ensuring high battery safety. All these properties make this nanocomposite a promising candidate anode material for room-temperature sodium-ion batteries for large-scale energy storage systems. In addition, this widely applicable spray drying method opens a new avenue in the improvement of low electronic conductivity electrode materials.

Acknowledgements

This work was supported by funding from the NSFC (51222210, 11234013), "973" Projects (2012CB932900), and One Hundred Talent Project of the Chinese Academy of Sciences.

Note and references

1 M. Armand, J. M. Tarascon, *Nature,* 2008, **451**, 652-657.

2 B. Dunn, H. Kamath, J. -M. Tarascon, *Science,* 2011, **334**, 928-935.

3 V. L. Chevrier, G. Ceder, *J. Electrochem. Soc*., 2011, **158**, A1011-A1014.

4 S. -W. Kim, D. -H. Seo, X. Ma, G. Ceder, K. Kang, *Adv. Energy Mater*., 2012, **2**, 710-721.

5 H. Pan, Y. -S. Hu, L. Chen, *Energy & Environ. Sci*., 2013, **6**, 2338-2360.

6 N. Yabuuchi, K. Kubota, M. Dahbi, S. Komaba, *Chem. Rev*., 2014, **114**, 11636-11682.

7 D. A. Stevens, J. R. Dahn, *J. Electrochem. Soc*., 2000, **147**, 1271-1273.

8 Y. Li, S. Xu, X. Wu, J. Yu, Y. Wang, Y. -S. Hu, H. Li, L. Chen, X. Huang, *J. Mater.*

Chem. A, 2015, **3**, 71-77.

9 J. Qian, Y. Chen, L. Wu, Y. Cao, X. Ai, H. Yang, *Chem. Commun*., 2012, **48**, 7070.

10 L. Xiao, Y. Cao, J. Xiao, W. Wang, L. Kovarik, Z. Nie, J. Liu, *Chem. Commun.,* 2012, **48**, 3321-3323.

11 P. Senguttuvan, G. Rousse, V. Seznec, J.-M. Tarascon, M.R. Palacín, *Chem. Mater*., 2011, **23**, 4109-4111.

12 H. Pan, X. Lu, X. Yu, Y. -S. Hu, H. Li, X. -Q. Yang, L. Chen, *Adv. Energy Mater.,* 2013, **3**, 1186-1194.

13 Y. Sun, L. Zhao, H. Pan, X. Lu, L. Gu, Y. -S. Hu, H. Li, M. Armand, Y. Ikuhara, L. Chen, X. Huang, *Nat. Commun.,* 2013, **4**, 1870.

14 Y. Wang, X. Yu, S. Xu, J. Bai, R. Xiao, Y. -S. Hu, H. Li, X. -Q. Yang, L. Chen, X. Huang, *Nat. Commun*., 2013, **4**, 2365.

15 S. I. Park, I. Gocheva, S. Okada, J. -i. Yamaki, *J. Electrochem. Soc.,* 2011, **158**, A1067-A1070.

16 P. Senguttuvan, G. Rousse, M. E. Arroyo y de Dompablo, H. Vezin, J. M. Tarascon, M. R. Palacín, *J. Am. Chem. Soc.,* 2013, **135**, 3897-3903.

17 H. Chen, M. Armand, G. Demailly, F. Dolhem, P. Poizot, J. -M. Tarascon, *Chemsuschem,* 2008, **1**, 348-355.

18 Y. Liang, Z. Tao, J. Chen, *Adv. Energy Mater*., 2012, **2**, 742-769.

19 Z. Song, H. Zhou, *Energy & Environ. Sci.,* 2013, **6**, 2280-2301.

20 W. Deng, X. Liang, X. Wu, J. Qian, Y. Cao, X. Ai, J. Feng, H. Yang, *Sci. Rep.,* 2013, **3**, 2671.

21 J. Hong, M. Lee, B. Lee, D. -H. Seo, C. B. Park, K. Kang, *Nat. Commun*., 2014, **5**, 5335.

22 L. Chen, W. Li, Y. Wang, C. Wang, Y. Xia, *RSC Adv.,* 2014, **4**, 25369-25375.

23 H. Chen, M. Armand, M. Courty, M. Jiang, C. P. Grey, F. Dolhem, J. -M. Tarascon, P. Poizot, *J. Am. Chem. Soc.,* 2009, **131**, 8984-8988.

24 R. -h. Zeng, X. -p. Li, Y. -c. Qiu, W. -s. Li, J. Yi, D. -s. Lu, C. -l. Tan, M. -q. Xu, *Electrochem. Commun.,* 2010, **12**, 1253-1256.

25 M. Armand, S. Grugeon, H. Vezin, S. Laruelle, P. Ribiere, P. Poizot, J. M.

Tarascon, *Nat. Mater.,* 2009, **8**, 120-125.

26 W. Walker, S. Grugeon, H. Vezin, S. Laruelle, M. Armand, J. M. Tarascon, F. Wudl, *Electrochem. Commun.,* 2010, **12**, 1348-1351.

27 L. Zhao, J. Zhao, Y. -S. Hu, H. Li, Z. Zhou, M. Armand, L. Chen, Adv. *Energy Mater.,* 2012, **2**, 962-965.

28 Y. Park, D. -S. Shin, S. H. Woo, N. S. Choi, K. H. Shin, S. M. Oh, K. T. Lee, S. Y. Hong, *Adv. Mater.,* 2012, **24**, 3562-3567.

29 A. Abouimrane, W. Weng, H. Eltayeb, Y. Cui, J. Niklas, O. Poluektov, K. Amine, *Energy & Environ. Sci.,* 2012, **5**, 9632-9638.

30 J. Xiang, C. Chang, M. Li, S. Wu, L. Yuan, J. Sun, *Crystal Growth & Design*, 2007, **8**, 280-282.

31 M. Yao, H. Senoh, S. -i. Yamazaki, Z. Siroma, T. Sakai, K. Yasuda, *J. Power Sources,* 2010, **195**, 8336-8340.

32 W. Walker, S. Grugeon, H. Vezin, S. Laruelle, M. Armand, F. Wudl, J.-M. Tarascon, *J. Mater. Chem.,* 2011, **21**, 1615-1620.

33 K. Bechgaard, V. D. Parker, *J. Am. Chem. Soc.,* 1972, **94**, 4749-4750.

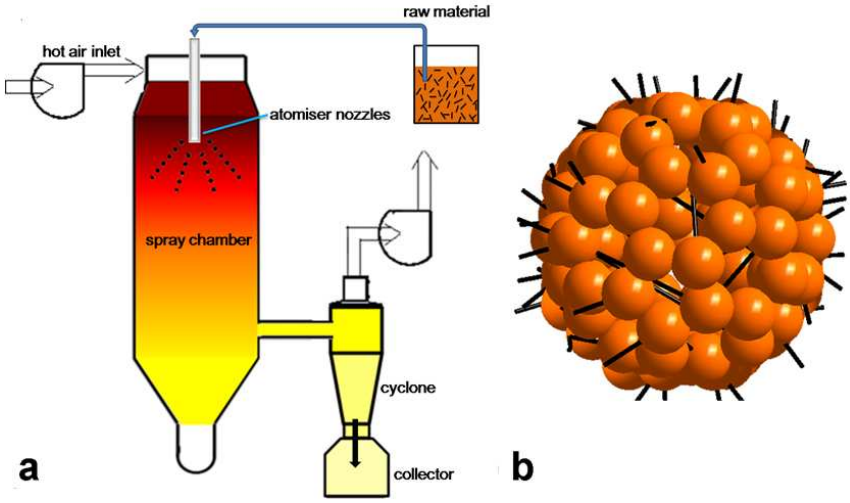

Figure 1. Spray drying granulation process. (a) The scheme of a spray dryer. (b) Schematic illustration of $Na_2C_6H_2O_4$/CNT nanocomposite.

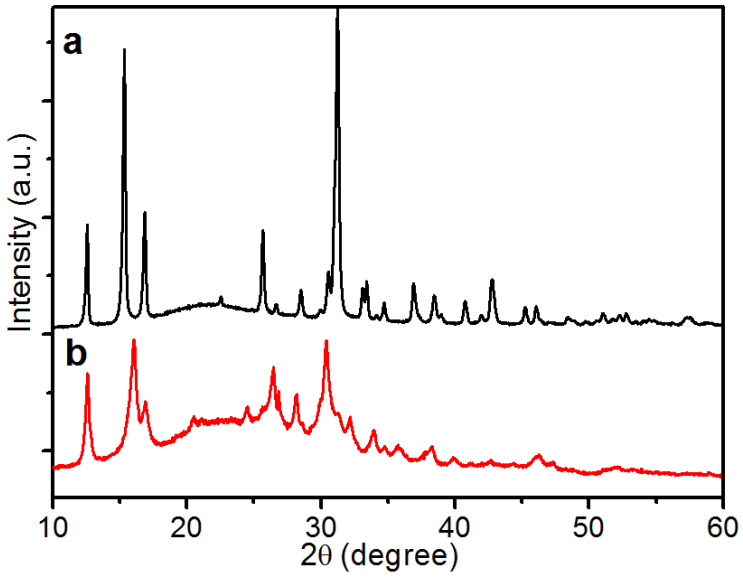

Figure 2. XRD patterns of (a) $Na_2C_6H_2O_4$ and (b) $Na_2C_6H_2O_4$/CNT nanocomposite.

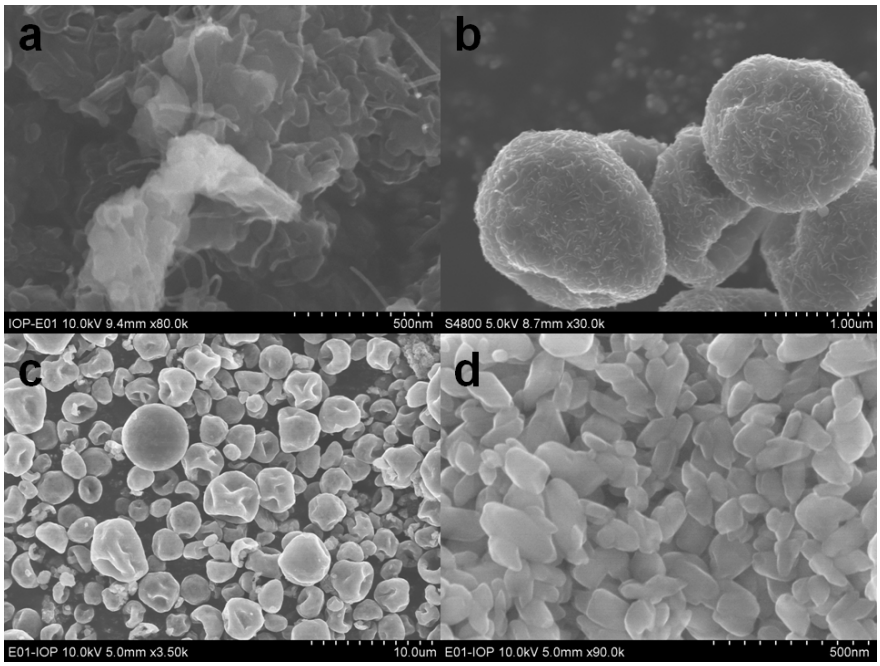

Figure 3. SEM images of $Na_2C_6H_2O_4$/CNT nanocomposite (a), (b), (c) in different magnifications and $Na_2C_6H_2O_4$ (d).

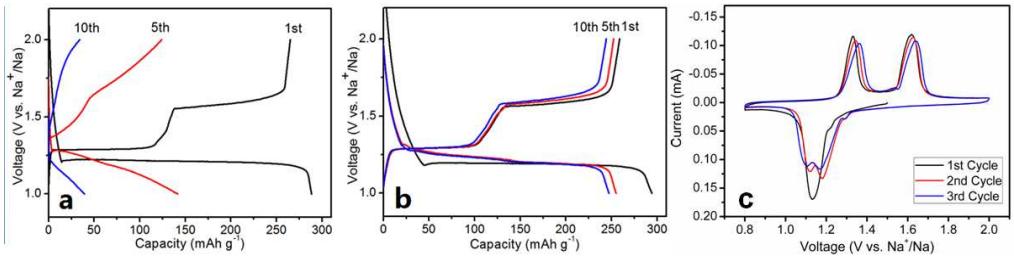

Figure 4. The 1st, 5th and 10th discharge/charge curves of (a) $Na_2C_6H_2O_4$ electrode and (b) $Na_2C_6H_2O_4$/CNT nanocomposite electrode at a current rate of C/10 (29 mA g^{-1}) in the voltage range of 1.0 and 2.0 V versus Na^+/Na. (c) The 1st, 2nd and 3rd cyclic voltammetry curves of $Na_2C_6H_2O_4$/CNT composite electrode at a scan rate of 0.03 mV s^{-1}.

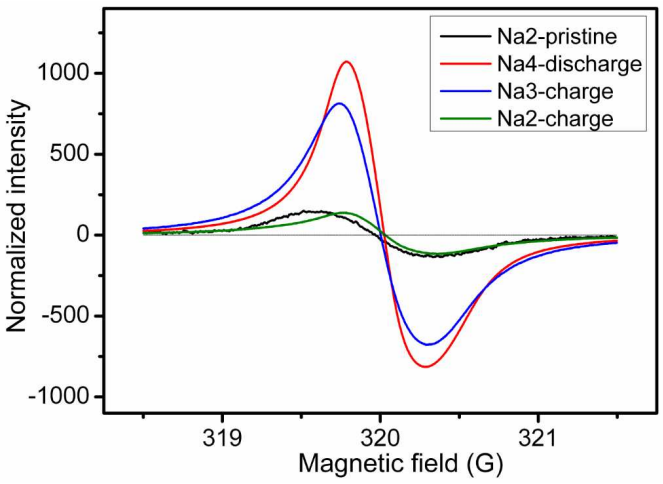

Figure 5. X-band EPR spectra recorded on $Na_2C_6H_2O_4$ electrodes at different discharge/charge states at room temperature.

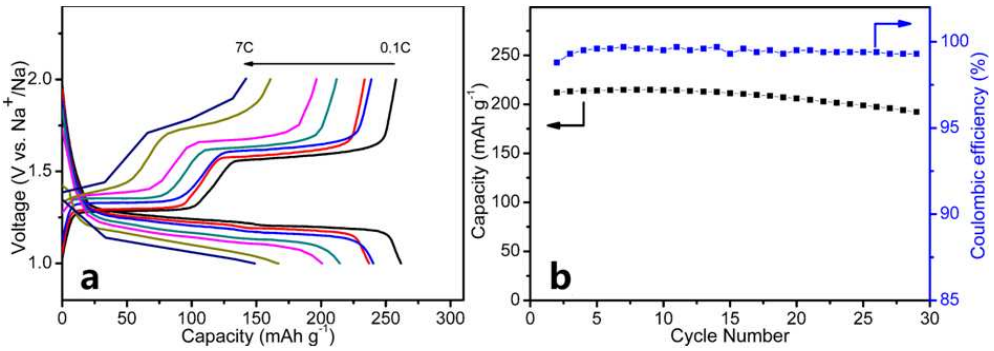

Figure 6. (a) Discharge/charge curves of $Na_2C_6H_2O_4$/CNT nanocomposite electrode at current rates of C/10, C/5, C/2, 1C, 2C, 5C and 7C. (b) Cycling performance. The capacity and Coulombic efficiency versus cycle number at a current rate of 1 C.